

Shot-to-shot displacement noise in state-expansion protocols with inverted potentials

Giuseppe Paolo Seta,^{1, 2} Louisiane Devaud,^{1, 2} Lorenzo Dania,^{1, 2} Lukas Novotny,^{1, 2} and Martin Frimmer^{1, 2}

¹*Photonics Laboratory, ETH Zürich, 8093 Zürich, Switzerland*

²*Quantum Center, ETH Zürich, 8093 Zürich, Switzerland*

(Dated: December 15, 2025)

Optically levitated nanoparticles are promising candidates for the generation of macroscopic quantum states of mechanical motion. Protocols to generate such states expose the particle to a succession of different potentials. Limited reproducibility of the alignment of these potentials across experimental realizations introduces additional noise. Here, we experimentally investigate and model how such shot-to-shot noise limits the coherence length of a levitated nanoparticle during a state-expansion protocol using a dark, inverted electrical potential. We identify electric stray fields and mechanical instabilities as major sources of shot-to-shot fluctuations. We discuss the resulting experimental requirements for state expansion protocols exploiting inverted potentials.

Introduction.— The superposition principle is at the heart of quantum mechanics. It gives rise to interference effects that challenge our intuition, especially for massive objects. For example, electrons, atoms, and even macromolecules, have been delocalized over distances much larger than their own size [1–5]. In a complementary approach, a mechanical mode of a comparatively massive crystal ($\sim 10^{17}$ atoms) has been observed in a superposition state, albeit of extremely small size ($\sim 10^{-18}$ m) [6]. Creating large superposition states of increasingly more massive systems is a prime goal of contemporary physics to test the limitations of quantum theory [7].

Optically levitated nanoparticles have been identified as a promising platform for this endeavor [8–13]. Mapping levitated systems onto the framework of optomechanics [14–16], and understanding how to best detect their motion [17, 18], have enabled cooling levitated oscillators to their motional ground state using optical cavities [19–21], and measurement-based feedback [22–24].

The extent of the ground-state wavefunction of a nanoparticle (diameter 100 nm) in a typical optical trap is around 10 pm [22, 23]. This small scale is a challenge for the generation of non-Gaussian states of motion [8, 9]. Such states require an anharmonic potential, which is currently not available on the minuscule length scale set by the zero-point fluctuations [25]. Protocols exploiting anharmonicities on larger length scales [26–28] envision inflating the wavefunction to a size where the non-parabolic nature of the potential is sizable [27–30].

Importantly, achieving a large spatial position uncertainty σ_z alone is not sufficient. Instead, preserving the quantum purity \mathcal{P} of the state throughout the expansion is essential, making the coherence length $\xi = \sqrt{8\mathcal{P}}\sigma_z$ the relevant figure of merit [8, 27]. The dominant source of decoherence in an optical trap in vacuum is photon recoil [31], which inspired proposals harnessing “dark” potentials that rely on electric or magnetic fields [26, 32].

On the experimental front, a number of efforts have been taken towards state expansion. All experiments initialize the particle in a tight optical trap, which is then either switched to a weaker confining potential [33, 34],

or switched off for free-evolution [35–39], or switched to an inverted configuration for exponentially accelerated expansion [40, 41]. Efforts entering the quantum regime thus far rely on purely optical potentials [34, 39]. Dark potentials, which promise expansion beyond the photon-recoil limit, have been used to expand thermal states of levitated nanoparticles in electrical confining and inverted configurations [33, 40]. This progress has been enabled by hybrid traps, combining optical levitation with ion-trapping technology [42–45].

Crucially, all protocols that expose the particle to different potentials require their repeatable alignment with sufficient precision [25]. Several proposals have recognized that a variation of this alignment (i.e., displacement noise) from one execution of the experiment to the next may limit demonstrations of quantum interference [26, 28, 46], and first evidence of this effect has recently surfaced in experiments with optical potentials [34]. In that light, it is surprising that no experimental study has systematically scrutinized displacement noise in levitation experiments, especially in configurations that deploy both bright and dark potentials.

In this work, we investigate shot-to-shot noise in a protocol expanding the motional state of an optically levitated nanoparticle in a dark inverted electrical potential. We find that mechanical instabilities and electrical stray forces limit the particle’s coherence length. Our model matches our experimental observations and reveals that shot-to-shot noise is different in nature as compared to white-noise. For currently available experimental parameters (initial coherence length 20 pm), reaching a coherence length of 1 nm requires a shot-to-shot displacement stability better than 0.5 pm. We discuss the challenges associated with shot-to-shot displacement noise in the context of levitodynamics, along with possible mitigation strategies.

Experimental details.— Figure 1(a) shows a sketch of the experimental setup, which consists of an optical trap and an electrical inverted potential. We trap single charged silica nanoparticles of nominal radius $R = 78$ nm, charge $|q| \approx 100e$, and mass $m \approx 4.4$ fg at pressure

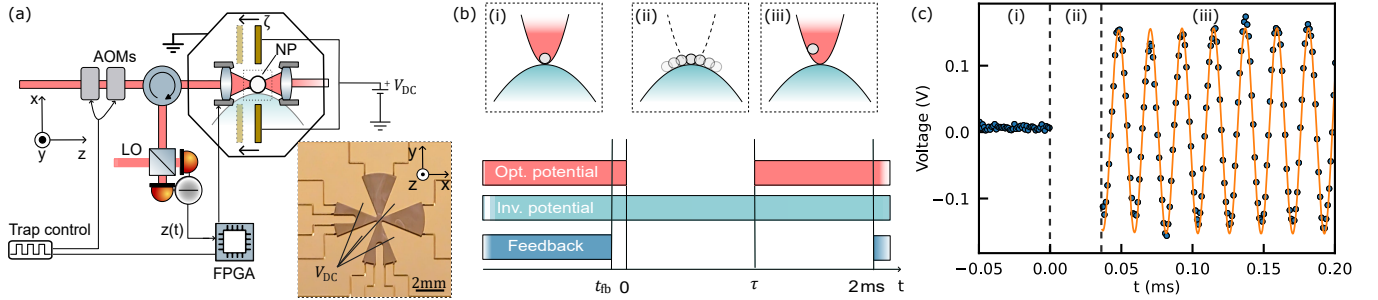


Figure 1. (a) Experimental setup. A nanoparticle (NP) is trapped by a focused laser beam in vacuum. The laser is toggled by two acousto-optic modulators (AOMs). The particle's motion is detected by mixing back-scattered light with a homodyne local oscillator (LO). The position signal is processed by a field-programmable gate array (FPGA) and used for feedback cooling. A planar chip with electrodes (see inset) is placed in the focal plane of the optical trap. The chip position ζ can be translated with a piezo stage (not shown). The electrodes are connected to a common static voltage V_{DC} , generating an inverted potential along the z axis. (b) State expansion protocol. Phase (i): Initialization in the optical potential, which dominates over the electrical potential, which is always on. Cooling is turned off at $t_{fb} = -1 \mu\text{s}$ before the optical trap is disabled at $t = 0$. Phase (ii): evolution in the inverted potential for a time τ . Phase (iii): recapture and measurement in the optical trap. (c) Detector time trace for a single realization of the protocol, where the particle evolves in the inverted potential for $\tau = 40 \mu\text{s}$. The raw trace is filtered (orange line) to estimate the recapture position $z(\tau)$ and momentum $p_z(\tau)$.

$p \approx 7 \times 10^{-7} \text{ mbar}$. The optical trap is generated by a laser (wavelength $\lambda = 1550 \text{ nm}$, power $P \approx 600 \text{ mW}$, optical axis along z , polarization along x , gravity along y) focused by an aspherical lens (numerical aperture NA = 0.8). The optical gradient force generates a three-dimensional harmonic potential for the c.m. motion of the trapped particle with trap frequencies $(\Omega_o^z, \Omega_o^x, \Omega_o^y) = 2\pi \times (44, 131, 150) \text{ kHz}$.

We detect the light backscattered by the particle [17] to apply linear feedback cooling to all three c.m. degrees of freedom to reduce their thermal population [47]. Throughout this work, we focus on the z mode. The lenses that focus and recollimate the trapping laser are mounted in conductive holders, which double as electrodes to apply a force along z to the charged nanoparticle. One of these electrodes applies an AC voltage for feedback cooling along the z axis, while the other is set to a constant potential to compensate for stray fields. Two acousto-optic modulators (AOMs) are used to turn the optical trap off and on, with a switching time of 200 ns.

The electric potential is generated by a micro-machined chip [45]. Four blade electrodes are carved out of a planar substrate (thickness 300 μm) and metallized. The separation between the tips of the electrodes and the nanoparticle is 250 μm . We apply a common static voltage V_{DC} to all four blade electrodes. Choosing the polarity of this voltage to match the polarity of the particle's net charge produces an anti-confining potential along the z axis and a confining potential in the xy plane. To leading order in z , the electric potential along the optical axis is an inverted harmonic potential $U = -m\Omega_{\text{inv}}^2 z^2$. The frequency Ω_{inv} characterizes the inverted potential curvature and is set by the voltage V_{DC} . The chip is mounted on a three-axis linear piezo stage to align the inverted electrical potential relative to the

optical trap.

We expand the motional state of the levitated particle along the z axis by evolution in the inverted electrical potential. To this end, we keep the electrical potential continuously on during the experiment, while the optical trap is switched off and on. When the optical trap is on, the anti-confining electrical potential along z superposes with the confining optical potential. The frequencies of the inverted electrical potential are always below $\Omega_{\text{inv}}/(2\pi) = 13 \text{ kHz}$, and therefore sufficiently small to lead to a net confining potential in presence of both the optical and the electrical potential.

Expansion protocol.— The experimental sequence for state expansion is composed of three phases, illustrated in Fig. 1(b). In phase (i), both the optical trap and the inverted electrical potential are engaged, leading to a net confining potential with frequency Ω_o^z . The particle is initialized by feedback cooling in the optical trap to a state with position variance σ_0^2 . In phase (ii), the optical trap is turned off and the particle evolves in the inverted electrical potential for a time τ . In phase (iii), the optical trap is switched back on and the particle is recaptured in the confining potential.

In Fig. 1(c), we plot an example of a measured position time trace of the particle along z for an evolution in the inverted potential for $\tau = 40 \mu\text{s}$. The position data during phase (i) represent the particle trajectory under feedback cooling. During phase (ii), the light field is off and no measurement record is available. Position data during phase (iii) hold information about the motional state of the particle after evolution in the inverted potential. We apply a retrodiction filter for times $t > \tau$ to optimally estimate the particle trajectory [33, 48]. From the filtered trace, we extract the recapture position $z(\tau)$ and momentum $p_z(\tau)$ in the optical trap at recapture

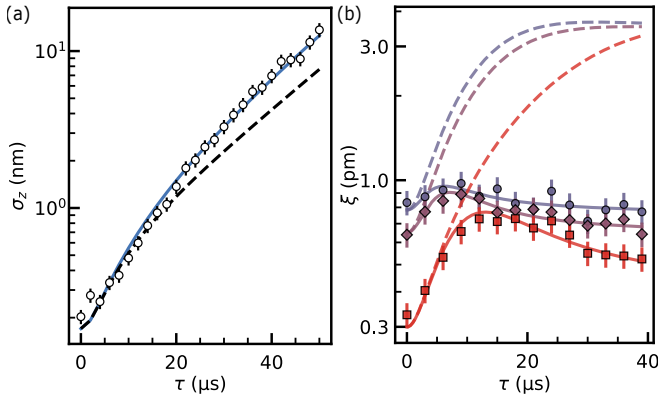


Figure 2. (a) Measured standard deviation of recapture positions σ_z as a function of expansion time τ . The black dashed line is the model restricted to Eqs. (1) and (2), i.e., in absence of shot-to-shot noise. The blue continuous line is a fit to our full model that includes shot-to-shot noise according to Eq. (3). (b) Inferred coherence length $\xi(\tau)$ for three different initial state sizes $\sigma_0 = 150$ pm (blue circles), $\sigma_0 = 187$ pm (purple diamonds), and $\sigma_0 = 384$ pm (red squares). The solid lines are fits to our full model including shot-to-shot noise. The dashed lines show the model prediction neglecting shot-to-shot noise.

time $t = \tau$. The protocol is repeated 200 times to acquire the mean position $\langle z \rangle$, momentum $\langle p_z \rangle$, their respective standard deviations σ_z and σ_{p_z} , as well as their covariance σ_{z,p_z}^2 at time τ .

To illustrate the expansion, Fig. 2(a) shows the measured standard deviation σ_z as a function of evolution time τ in an inverted potential with frequency $\Omega_{\text{inv}} = 2\pi \times 9.3 kHz. The value of σ_z expands from $\sigma_z(0) = (202 \pm 21)$ pm (≈ 450 phonons) up to $\sigma_z(50 \mu\text{s}) = (13.70 \pm 1.42)$ nm, corresponding to an increase by 37 dB in variance.$

For future experiments in the quantum regime, the relevant quantity is not the total position uncertainty σ_z , but rather its coherent part, which is quantified by the coherence length $\xi = \sqrt{8\mathcal{P}\sigma_z}$ [8]. For a Gaussian state, the purity is given by $\mathcal{P} = \hbar/[2(\sigma_z^2\sigma_{p_z}^2 - \sigma_{zp_z}^4)^{1/2}]$. It measures how far the state is from the Heisenberg bound. In Fig. 2(b), we show as blue circles the coherence length ξ inferred from our measurements as a function of τ for an inverted potential with frequency $\Omega_{\text{inv}} = 2\pi \times 7.6$ kHz starting from an initial state size $\sigma_0 = 150$ pm (corresponding to an initial coherence length $\xi_0 = 0.83$ pm). The inferred coherence length slightly increases with increasing τ , reaching a maximum of 0.97 pm, before decaying. As a second example (red squares), we show the same experiment with a larger initial state size $\sigma_0 = 384$ pm (corresponding to $\xi_0 = 0.33$ pm). This larger state size is obtained by reducing the gain of the feedback cooling. The inferred coherence length of this comparably hot state expands to $\xi = 0.73$ pm in the inverted potential before decaying. We show a third dataset with

an intermediate starting state size $\sigma_0 = 187$ pm [purple diamonds].

White noise heating.— We proceed by comparing our measurements to the currently established model for the state size σ_z and coherence length ξ [33, 40]. The total variance $\sigma_z^2(\tau) = \sigma_{\text{coh}}^2(\tau) + \sigma_{\text{wn}}^2(\tau)$ is the sum of two terms. The coherent part

$$\sigma_{\text{coh}}^2(\tau) = \sigma_0^2 [\cosh^2(\Omega_{\text{inv}}\tau) + r^2 \sinh^2(\Omega_{\text{inv}}\tau)] \quad (1)$$

represents the desired expansion of the initial variance σ_0^2 in the inverted potential, where $r = \Omega_z^2/\Omega_{\text{inv}}$ is the ratio of the confining and inverted potential frequencies. The incoherent part

$$\sigma_{\text{wn}}^2(\tau) = \frac{r\hbar\Gamma}{m\Omega_{\text{inv}}} \left[\frac{\sinh(2\Omega_{\text{inv}}\tau)}{2\Omega_{\text{inv}}} - \tau \right] \quad (2)$$

represents added position variance due to white-noise heating by a thermal bath at a rate Γ (measured in units of phonons of the optical potential). In practice, Γ stems from photon recoil and gas collisions. For our system, from an independent reheating measurement [47], we extract $\Gamma = 2\pi \times 554$ kHz, matching the value expected from collisions with gas molecules at the measured pressure.

To compare theory and experiment, we plot (black dashed line) in Fig. 2(a) the calculated standard deviation σ_z from Eqs. (1) and (2) using the measured value for Γ and $\sigma_0 = 170$ pm. The measured position standard deviation exceeds the one predicted by coherent expansion and white-noise heating. Even more striking is the result when adding the model prediction for the coherence length to Fig. 2(b). The model (dashed lines) clearly overestimates the experimentally inferred coherence length at long times, suggesting an additional source of noise not accounted for by the model.

A particularly revealing feature in Fig. 2(b) is that the experimentally inferred coherence lengths at large τ approach different values for different initial coherence lengths ξ_0 . In contrast, state expansion in an inverted potential under white-noise heating drives the coherence length to a value that is independent of the initial coherence length. This can be observed in Fig. 2(b), where the dashed lines asymptotically approach the same value at large τ . Therefore, our results speak against the validity of any model that considers only white-noise heating.

In the following, we provide evidence that the observed additional noise is due to shot-to-shot fluctuations of the relative alignment of the optical and the effective electrical potential.

Shot-to-shot displacement noise.— When the relative displacement between the inverted potential and the confining potential is constant during a single realization of the expansion protocol, but varies between realizations, the additional shot-to-shot position variance

$$\sigma_{\text{shot}}^2 = \sigma_{\text{disp}}^2 (r^{-2} + 1)^2 [1 - \cosh(\Omega_{\text{inv}}\tau)]^2 \quad (3)$$

contributes to the state size, where σ_{disp}^2 is the shot-to-shot variance of the spatial displacement between optical and inverted potential (see Supplement for derivation [49]).

We return to the data in Fig. 2(b) and fit each dataset to our full model with σ_0 and σ_{disp} as the only free parameters (solid lines). For σ_{disp} , we obtain the values 3.68 ± 0.53 nm (circles), 3.38 ± 0.42 nm (diamonds), and 2.27 ± 0.12 nm (squares). The agreement between the measured data and the fit strongly supports our hypothesis that shot-to-shot noise makes a significant contribution in our experiments. Also the measured position standard deviation in Fig. 2(a) matches our full model (blue solid line) with the fit parameters $\sigma_{\text{disp}} = (1.14 \pm 0.07)$ nm and $\sigma_0 = (170 \pm 8)$ pm.

We continue by identifying the different contributions to the shot-to-shot displacement noise σ_{disp} . First, an electric stray field acts as a Coulomb force on the particle. This stray force effectively shifts the optical and the electrical potential relative to each other. We denote the shot-to-shot variance of this electrical stray force by σ_{sf}^2 . Second, the position of the electrical potential, set by the position of the chip relative to the optical potential (quantified by their distance ζ), can fluctuate, which is quantified by the shot-to-shot chip-position variance σ_ζ^2 . Assuming uncorrelated chip-position and stray-force fluctuations, the effective displacement variance is

$$\sigma_{\text{disp}}^2 = \sigma_{\text{sf}}^2(m\Omega_{\text{inv}}^2)^{-2} + \sigma_\zeta^2. \quad (4)$$

In the first term, the force fluctuations are transduced into position fluctuations by the spring constant of the inverted potential.

To individually quantify σ_{sf} and σ_ζ , we repeat the experiment in Fig. 2(a) for different values of the inverted potential frequency Ω_{inv} . We plot the obtained values of σ_{disp} as a function of Ω_{inv} in Fig. 3(a) and observe that σ_{disp} drops with increasing Ω_{inv} . To quantify the different shot-to-shot noise contributions, we fit (dashed line) the data to Eq. (4), and extract the parameters $\sigma_{\text{sf}} = (10.9 \pm 0.5)$ aN and $\sigma_\zeta = (834 \pm 53)$ pm. We conclude that σ_{disp} is dominated by stray force fluctuations for small Ω_{inv} , whereas mechanical position fluctuations prevail for large Ω_{inv} .

Discussion.— We now use our model to assess the noise conditions required for expanding the motional state of a levitated nanoparticle to dimensions comparable to the particle size. In Fig. 3(b), we show a false-color plot of the maximally achievable coherence length ξ_{max} for an expansion of a particle in its ground-state (zero-point size $\sigma_0 = 7$ pm, corresponding optical trap frequency $\Omega_o = 2\pi \times 40$ kHz) in an inverted potential with frequency $\Omega_{\text{inv}} = 2\pi \times 10$ kHz as a function of σ_{disp} and Γ . We observe that reaching $\xi_{\text{max}} = 1$ nm requires $\Gamma/(2\pi) < 1$ Hz and $\sigma_{\text{disp}} < 0.5$ pm. Therefore, expanding the coherence length to $\xi \sim 50\xi_0$ requires a shot-to-shot displacement noise that is ~ 50 times smaller than

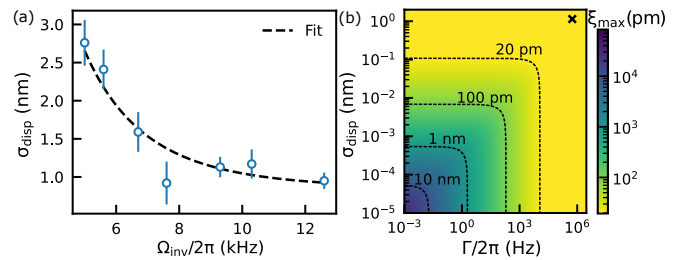


Figure 3. (a) Measured σ_{disp} as function of Ω_{inv} . Error bars indicate uncertainty of the fit used for extraction. The dashed line is a fit of the data to Eq. (4). (b) False-color plot of calculated maximally achievable coherence length ξ_{max} as a function of σ_{disp} and Γ . We fix $\sigma_0 = 7$ pm, $\Omega_o = 2\pi \times 40$ kHz and $\Omega_{\text{inv}} = 2\pi \times 10$ kHz. Dotted lines are contours for the indicated coherence lengths. The black cross represents the values of σ_{disp} and Γ for the measurement in Fig. 2(a).

the initial coherence length ($\sigma_{\text{disp}} \lesssim \xi_0/50$). This value is comparable to the stability requirement obtained by analyzing the visibility of interference fringes in an all-optical interference protocol [28]. Regarding the scaling, an enhancement of ξ_{max} by one order of magnitude requires an improvement of σ_{disp} by roughly one order of magnitude and Γ by two orders of magnitude.

We can now deduce technical requirements. For white-noise heating by electric fields, the voltage-noise spectral density required for a desired Γ , at a given electrode distance d , can be estimated as $S_v = 2d^2\Gamma\hbar m\Omega_o/q^2$ [50]. To achieve $\Gamma/(2\pi) = 1$ Hz with our particle and assuming $d = 1$ mm, we obtain $S_v \approx 6$ nV/ $\sqrt{\text{Hz}}$. This value is comparable to 10 nV/ $\sqrt{\text{Hz}}$, achievable in practice [51, 52].

Let us turn to the shot-to-shot noise σ_{disp} and its two contributions σ_ζ and σ_{sf} . For the mechanical shot-to-shot fluctuations σ_ζ to remain below 0.5 pm in a bandwidth set by a realistically required duration of the expansion of $\tau_{\text{ex}} = 100$ μ s requires a position noise level $S_{\zeta\zeta} = 2\tau_{\text{ex}}(0.5 \text{ pm})^2 \approx 10^{-28} \text{ m}^2 \text{ Hz}^{-1}$ in the low frequency range. Encouraging experiments with superconductive traps and levitated magnetic particles have demonstrated mechanical noise down to $10^{-27} \text{ m}^2 \text{ Hz}^{-1}$ in the few-Hertz range [53]. Following the same reasoning, low-frequency stray forces have to be suppressed to a noise level of $S_{\text{sf}} = 2\tau_{\text{ex}}(m\Omega_{\text{inv}}^2 \times 0.5 \text{ pm})^2 \approx 10^{-44} \text{ N}^2 \text{ Hz}^{-1}$ for $\Omega_{\text{inv}} = 2\pi \times 10$ kHz. To achieve the required S_{sf} , it is crucial to understand the stray force origin. We suspect that the main contribution to σ_{sf} stems from charge fluctuations of dielectric surfaces in close proximity to the particle, such as the trapping and collection lenses [35, 50, 54, 55]. These fluctuations may be reduced by coating the lens surfaces with conductive transparent materials.

Besides passively reducing stray fields and mechanical instabilities, one can envision measuring their instantaneous values at each shot of the experiment to either correct for them actively or in post-processing. Further-

more, dedicated protocols to cancel shot-to-shot noise in expansion protocols developed for confining traps may find adaptations for inverted potentials [34].

Finally, we comment on the choice of inverted trap frequency, which is not straightforward in the parameter range of interest (see Supplement for details [49]). In the absence of shot-to-shot fluctuations, where noise is purely due to white-noise heating, it is always beneficial to maximally accelerate the expansion dynamics by choosing Ω_{inv} large. In contrast, in the presence of shot-to-shot noise, larger Ω_{inv} leads to a reduction in maximally achievable coherence length for constant Γ and σ_{inv} . Thus, for displacement noise from electrode position fluctuations [σ_ζ in Eq. (4)], higher Ω_{inv} is undesirable. However, the contribution of stray forces in Eq. (4) is reduced by the inverse trap frequency Ω_{inv}^4 . Thus, when limited by stray forces, increasing Ω_{inv} is beneficial. Therefore, a quantitative characterization of the different sources of noise is required to optimally choose experimental parameters.

Conclusions.— We have experimentally quantified the sources of noise acting on a levitated nanoparticle during a state-expansion protocol in a dark inverted potential. Besides white-noise heating, we have identified shot-to-shot displacement fluctuations between experimental repetitions as the dominant limitation of the coherence length. These shot-to-shot fluctuations have contributions from mechanical motion of the chip holding the electrodes, and from fluctuations of electric stray fields. Our model for shot-to-shot noise is supported by our experimental findings. With this model, we have quantified the required shot-to-shot stability for reaching coherence lengths in the nanometer range. The relevance of our work extends across the diverse communities harnessing levitated nanoparticles in vacuum. It provides a starting point for the experimental progress that will be required to enable matter-wave experiments using optical and electrical potentials [8–10, 26, 28]. This progress will also benefit the communities aiming to exploit squeezed states of levitated motion for quantum sensing [29, 30, 34, 39], as well as endeavors aiming to couple levitated nanoparticles to other quantum systems, such as free electrons [12] or two-level systems [11, 13]. Finally, this work may serve as a platform to interface with the quantum-simulation community, currently facing shot-to-shot noise as a serious technical concern [56].

Acknowledgments.— This research has been supported by the Swiss SERI Quantum Initiative (grants no. UeM019-2 and no. UeM029-3), by the Swiss National Science Foundation (grant no. 212599), and by the European Research Council (ERC) under grant agreement no. 951234 (Q-Xtreme ERC 2020-SyG). L. Dania acknowledges support from the Quantum Center Research Fellowship and the Dr Alfred and Flora Späli Fonds. L. Devaud thanks for support through her SNSF Fellowship (TMPFP2_217122). We thank the participants of

the Q-Xtreme retreats as well as C. Dellago for fruitful discussions.

- [1] C. Davisson and L. H. Germer, The scattering of electrons by a single crystal of nickel, *Nature* **119**, 558 (1927).
- [2] C. Monroe, D. M. Meekhof, B. E. King, and D. J. Wineland, A “schrödinger cat” superposition state of an atom, *Science* **272**, 1131 (1996).
- [3] T. Schumm, S. Hofferberth, L. M. Andersson, S. Wildermuth, S. Groth, I. Bar-Joseph, J. Schmiedmayer, and P. Krüger, Matter-wave interferometry in a double well on an atom chip, *Nature Physics* **1**, 57 (2005).
- [4] K. Hornberger, S. Gerlich, P. Haslinger, S. Nimmrichter, and M. Arndt, Colloquium: Quantum interference of clusters and molecules, *Rev. Mod. Phys.* **84**, 157 (2012).
- [5] Y. Y. Fein, P. Geyer, P. Zwick, F. Kiaika, S. Pedalino, M. Mayor, S. Gerlich, and M. Arndt, Quantum superposition of molecules beyond 25 kda, *Nature Physics* **15**, 1242 (2019).
- [6] M. Bild, M. Fadel, Y. Yang, U. von Lüpke, P. Martin, A. Bruno, and Y. Chu, Schrödinger cat states of a 16-microgram mechanical oscillator, *Science* **380**, 274 (2023).
- [7] A. Bassi, K. Lochan, S. Satin, T. P. Singh, and H. Ulbricht, Models of wave-function collapse, underlying theories, and experimental tests, *Rev. Mod. Phys.* **85**, 471 (2013).
- [8] O. Romero-Isart, Quantum superposition of massive objects and collapse models, *Phys. Rev. A* **84**, 052121 (2011).
- [9] O. Romero-Isart, A. C. Pflanzer, F. Blaser, R. Kaltenbaek, N. Kiesel, M. Aspelmeyer, and J. I. Cirac, Large quantum superpositions and interference of massive nanometer-sized objects, *Phys. Rev. Lett.* **107**, 020405 (2011).
- [10] J. Bateman, S. Nimmrichter, K. Hornberger, and H. Ulbricht, Near-field interferometry of a free-falling nanoparticle from a point-like source, *Nature Communications* **5**, 4788 (2014).
- [11] C. Wan, M. Scala, G. W. Morley, A. A. Rahman, H. Ulbricht, J. Bateman, P. F. Barker, S. Bose, and M. S. Kim, Free nano-object ramsey interferometry for large quantum superpositions, *Phys. Rev. Lett.* **117**, 143003 (2016).
- [12] S. Nimmrichter, D. Rätzel, I. C. Bicket, M. S. Seifner, and P. Haslinger, Electron-enabled nanoparticle diffraction, *Phys. Rev. Lett.* **135**, 173601 (2025).
- [13] D. S. Bykov, L. Dania, F. Goschin, and T. E. Northup, Nanoparticle stored with an atomic ion in a linear paul trap, *Phys. Rev. Lett.* **135**, 213602 (2025).
- [14] O. Romero-Isart, A. C. Pflanzer, M. L. Juan, R. Quidant, N. Kiesel, M. Aspelmeyer, and J. I. Cirac, Optically levitating dielectrics in the quantum regime: Theory and protocols, *Phys. Rev. A* **83**, 013803 (2011).
- [15] D. E. Chang, C. A. Regal, S. B. Papp, D. J. Wilson, J. Ye, O. Painter, H. J. Kimble, and P. Zoller, Cavity opto-mechanics using an optically levitated nanosphere, *Proceedings of the National Academy of Sciences* **107**, 1005 (2010).

[16] M. Aspelmeyer, T. J. Kippenberg, and F. Marquardt, Cavity optomechanics, *Rev. Mod. Phys.* **86**, 1391 (2014).

[17] F. Tebbenjohanns, M. Frimmen, and L. Novotny, Optimal position detection of a dipolar scatterer in a focused field, *Phys. Rev. A* **100**, 043821 (2019).

[18] F. Tebbenjohanns, M. Frimmen, V. Jain, D. Windey, and L. Novotny, Motional sideband asymmetry of a nanoparticle optically levitated in free space, *Phys. Rev. Lett.* **124**, 013603 (2020).

[19] U. Delić, M. Reisenbauer, K. Dare, D. Grass, V. Vuletić, N. Kiesel, and M. Aspelmeyer, Cooling of a levitated nanoparticle to the motional quantum ground state, *Science* **367**, 892 (2020).

[20] J. Piotrowski, D. Windey, J. Vijayan, C. Gonzalez-Ballester, A. de los Ríos Sommer, N. Meyer, R. Quidant, O. Romero-Isart, R. Reimann, and L. Novotny, Simultaneous ground-state cooling of two mechanical modes of a levitated nanoparticle, *Nature Physics* **19**, 1009 (2023).

[21] A. Ranfagni, K. Børkje, F. Marino, and F. Marin, Two-dimensional quantum motion of a levitated nanosphere, *Phys. Rev. Res.* **4**, 033051 (2022).

[22] L. Magrini, P. Rosenzweig, C. Bach, A. Deutschmann-Olek, S. G. Hofer, S. Hong, N. Kiesel, A. Kugi, and M. Aspelmeyer, Real-time optimal quantum control of mechanical motion at room temperature, *Nature* **595**, 373–377 (2021).

[23] F. Tebbenjohanns, M. L. Mattana, M. Rossi, M. Frimmen, and L. Novotny, Quantum control of a nanoparticle optically levitated in cryogenic free space, *Nature* **595**, 378 (2021).

[24] M. Kamba, R. Shimizu, and K. Aikawa, Optical cold damping of neutral nanoparticles near the ground state in an optical lattice, *Opt. Express* **30**, 26716 (2022).

[25] C. Gonzalez-Ballester, M. Aspelmeyer, L. Novotny, R. Quidant, and O. Romero-Isart, Levitodynamics: Levitation and control of microscopic objects in vacuum, *Science* **374**, eabg3027 (2021).

[26] M. Roda-Llordes, A. Riera-Campeny, D. Candoli, P. T. Grochowski, and O. Romero-Isart, Macroscopic quantum superpositions via dynamics in a wide double-well potential, *Phys. Rev. Lett.* **132**, 023601 (2024).

[27] O. Romero-Isart, Coherent inflation for large quantum superpositions of levitated microspheres, *New Journal of Physics* **19**, 123029 (2017).

[28] L. Neumeier, M. A. Ciampini, O. Romero-Isart, M. Aspelmeyer, and N. Kiesel, Fast quantum interference of a nanoparticle via optical potential control, *Proceedings of the National Academy of Sciences* **121**, e2306953121 (2024).

[29] T. Weiss, M. Roda-Llordes, E. Torrontegui, M. Aspelmeyer, and O. Romero-Isart, Large quantum delocalization of a levitated nanoparticle using optimal control: Applications for force sensing and entangling via weak forces, *Phys. Rev. Lett.* **127**, 023601 (2021).

[30] F. Cosco, J. S. Pedernales, and M. B. Plenio, Enhanced force sensitivity and entanglement in periodically driven optomechanics, *Phys. Rev. A* **103**, L061501 (2021).

[31] V. Jain, J. Gieseler, C. Moritz, C. Dellago, R. Quidant, and L. Novotny, Direct measurement of photon recoil from a levitated nanoparticle, *Phys. Rev. Lett.* **116**, 243601 (2016).

[32] H. Pino, J. Prat-Camps, K. Sinha, B. P. Venkatesh, and O. Romero-Isart, On-chip quantum interference of a superconducting microsphere, *Quantum Science and Technology* **3**, 025001 (2018).

[33] E. Bonvin, L. Devaud, M. Rossi, A. Militaru, L. Dania, D. S. Bykov, O. Romero-Isart, T. E. Northup, L. Novotny, and M. Frimmen, State expansion of a levitated nanoparticle in a dark harmonic potential, *Phys. Rev. Lett.* **132**, 253602 (2024).

[34] M. Rossi, A. Militaru, N. Carlon Zambon, A. Riera-Campeny, O. Romero-Isart, M. Frimmen, and L. Novotny, Quantum delocalization of a levitated nanoparticle, *Phys. Rev. Lett.* **135**, 083601 (2025).

[35] E. Hebestreit, M. Frimmen, R. Reimann, and L. Novotny, Sensing static forces with free-falling nanoparticles, *Phys. Rev. Lett.* **121**, 063602 (2018).

[36] M. L. Mattana, N. C. Zambon, M. Rossi, E. Bonvin, L. Devaud, M. Frimmen, and L. Novotny, *Trap-to-trap free falls with an optically levitated nanoparticle* (2025), arXiv:2507.12995 [quant-ph].

[37] D. Steiner, Y. Y. Fein, G. Meier, S. Lindner, P. Juschitz, M. A. Ciampini, M. Aspelmeyer, and N. Kiesel, Free expansion of a charged nanoparticle via electrostatic compensation, *Applied Physics Letters* **127**, 191103 (2025).

[38] M. Kamba and K. Aikawa, Revealing the velocity uncertainties of a levitated particle in the quantum ground state, *Phys. Rev. Lett.* **131**, 183602 (2023).

[39] M. Kamba, N. Hara, and K. Aikawa, Quantum squeezing of a levitated nanomechanical oscillator, *Science* **389**, 1225 (2025).

[40] G. F. M. Tomassi, D. Veldhuizen, B. Melo, D. Candoli, A. Riera-Campeny, O. Romero-Isart, N. Meyer, and R. Quidant, *Accelerated state expansion of a nanoparticle in a dark inverted potential* (2025), arXiv:2503.20707 [quant-ph].

[41] M. Duchaň, M. Šiler, P. Jákl, O. Brzobohatý, A. Rakhubovsky, R. Filip, and P. Zemánek, Nanomechanical state amplifier based on optical inverted pendulum, *Communications Physics* **8**, 276 (2025).

[42] G. P. Conangla, A. W. Schell, R. A. Rica, and R. Quidant, Motion control and optical interrogation of a levitating single nitrogen vacancy in vacuum, *Nano Letters* **18**, 3956 (2018).

[43] G. P. Conangla, R. A. Rica, and R. Quidant, Extending vacuum trapping to absorbing objects with hybrid paul-optical traps, *Nano Letters* **20**, 6018 (2020).

[44] D. S. Bykov, M. Meusburger, L. Dania, and T. E. Northup, Hybrid electro-optical trap for experiments with levitated particles in vacuum, *Review of Scientific Instruments* **93**, 073201 (2022).

[45] E. Bonvin, L. Devaud, M. Rossi, A. Militaru, L. Dania, D. S. Bykov, M. Teller, T. E. Northup, L. Novotny, and M. Frimmen, Hybrid paul-optical trap with large optical access for levitated optomechanics, *Phys. Rev. Res.* **6**, 043129 (2024).

[46] J. S. Pedernales and M. B. Plenio, Robust macroscopic matter-wave interferometry with solids, *Phys. Rev. A* **105**, 063313 (2022).

[47] F. Tebbenjohanns, M. Frimmen, A. Militaru, V. Jain, and L. Novotny, Cold damping of an optically levitated nanoparticle to microkelvin temperatures, *Phys. Rev. Lett.* **122**, 223601 (2019).

[48] M. Rossi, D. Mason, J. Chen, and A. Schliesser, Observing and verifying the quantum trajectory of a mechanical resonator, *Phys. Rev. Lett.* **123**, 163601 (2019).

[49] Supplemental material for this paper, URL: [to be inserted by publisher], contains the derivation of the model

and a discussion of the role of Ω_{inv} for maximal coherence length.

[50] M. Brownnutt, M. Kumph, P. Rabl, and R. Blatt, Ion-trap measurements of electric-field noise near surfaces, *Rev. Mod. Phys.* **87**, 1419 (2015).

[51] L. Dania, D. S. Bykov, F. Goschin, M. Teller, A. Kassid, and T. E. Northup, Ultrahigh quality factor of a levitated nanomechanical oscillator, *Phys. Rev. Lett.* **132**, 133602 (2024).

[52] A. Vinante, A. Pontin, M. Rashid, M. Toroš, P. F. Barker, and H. Ulbricht, Testing collapse models with levitated nanoparticles: Detection challenge, *Phys. Rev. A* **100**, 012119 (2019).

[53] T. M. Fuchs, D. G. Uitenbroek, J. Plugge, N. van Halteren, J.-P. van Soest, A. Vinante, H. Ulbricht, and T. H. Oosterkamp, Measuring gravity with milligram levitated masses, *Science Advances* **10**, eadk2949 (2024).

[54] M. Teller, D. A. Fioretto, P. C. Holz, P. Schindler, V. Messerer, K. Schüppert, Y. Zou, R. Blatt, J. Chiaverini, J. Sage, and T. E. Northup, Heating of a trapped ion induced by dielectric materials, *Phys. Rev. Lett.* **126**, 230505 (2021).

[55] T. Sägesser, S. Jain, P. Hrmo, A. Ferk, M. Simoni, Y. Cui, C. Mordini, D. Kienzler, and J. Home, A 3-dimensional scanning trapped-ion probe (2024), [arXiv:2412.17528 \[quant-ph\]](https://arxiv.org/abs/2412.17528).

[56] T. Steckmann, D. Luo, Y.-X. Wang, S. R. Muleady, A. Seif, C. Monroe, M. J. Gullans, A. V. Gorshkov, O. Katz, and A. Schuckert, Error mitigation of shot-to-shot fluctuations in analog quantum simulators (2025), [arXiv:2506.16509](https://arxiv.org/abs/2506.16509).